

# Large Eddy Simulation Applied on the Analysis of Vortex Tube

Million Asfaw Belay

**Abstract**— This paper deals with the work carried out in Ranque-Hilsch vortex tube (RHVT). The gas is injected tangentially into a nozzle chamber with high degree of swirl velocity so that air travels in a spiral motion along the periphery of the hot side. A three dimensional RHVT model is constructed and used to carry out the numerical computation in the framework of commercial CFD code Fluent for predicting the energy separation and flow phenomenon inside the tube. Moreover, five turbulence models including standard k-epsilon (sk- $\epsilon$ ), renormalization group k-epsilon (RNG k- $\epsilon$ ), k-omega (k- $\omega$ ), Reynolds stress model (RSM) and large eddy simulation (LES) model are adopted in the calculating procedures for evaluating their outcomes. As a result, the numerical simulations clearly illustrate the temperature separation and flow phenomena within the vortex tube. Also, the CFD flow visualization on vortex tube can identify three regions, which are the incoming fluid at ambient temperature and high pressure, the cold exit and the hot exit where the temperatures are significant lower or higher than the inlet temperature, respectively. Also, performance curves (cold temperature separation versus cold outlet mass fraction) of vortex tube were obtained successfully under a given inlet pressure. Regards the comparison among turbulent models, CFD predictions from the large eddy simulation yields the best high-resolution flow pattern and provides more detailed information for understanding the physical mechanisms of this flow and energy separation. Also, its calculated results are in a better agreement with the available experimental measurements compared to other turbulent models.

**Index Terms**— Ranque-Hilsch vortex tube, CFD code Fluent, sk- $\epsilon$ , RNGk- $\epsilon$ , k- $\omega$ , RSM and LES

## I. INTRODUCTION

An external analysis proves that the RHVT obeys both the First and Second Laws of Thermodynamics. However this external analysis does not offer any insight into the internal mechanisms of the RHVT which force the temperature separations to both the hot and cold outlets. Despite the simplicity of the vortex tubes geometry, the energy separation phenomenon within the RHVT is quite complex. At present several conflicting theories have been advanced to explain the vortex tubes behavior since its initial observation by Ranque [1]. He explained Heat supplying process takes place by the inner sheet of fluid expanding so as to compressing the outer sheet of fluid. Hilsch [2] designed the vortex tube for better efficiency and hypothesized the expansion of a gas in a centrifugal field producing cold gas and heating of gas due to friction to yield the temperature separation. Scheper [5] found that the static temperature decreased in a radially outward direction. He hypothesized the energy separation mechanism as heat transfer by forced convection. Martynovskii and

Alekseev [6] obtained the analytic expression for the ratio of kinetic energy and heat currents and conducted experiment to verify a hypothesis. They argued that temperature separation is obtained due to work transfer from core to periphery. Bruun [7] measured the velocity distribution of air in a counter flow vortex tube at various cross-sections. Comparison is made between the order of magnitude of the radial and axial convection terms in the equations of motion and energy. He argued that turbulent heat transport could lead to temperature separation. Yunpeng Xue et al. [8] have shown that the energy separation in the vortex tube seems to involve a number of different factors, among which expansion and friction between the flow layers could be considered as the most important.

Recently, computational fluid dynamics (CFD) modeling has been successfully utilized to explain the fundamental principles behind energy separation. Promvonge [9] used an algebraic Reynolds stress model (ASM) and the k- $\epsilon$  turbulence model for CFD simulation of the flow phenomena in a vortex tube. He observed a better prediction of temperature separation by the ASM over the k- $\epsilon$  turbulence model. Frohlingsdorf and Unger [10] presented a CFD model of energy separation by considering compressibility and turbulence effects. They used the CFX code with the k- $\epsilon$  turbulence model. Behera et al. [11] presented a three dimensional CFD model for analysis of energy separation using code system STAR CD with the RNG k- $\epsilon$  turbulence model. They investigated the effect of shape, size and number of nozzles on temperature separation in the vortex tube. Aljuwayhel et al. [4] investigated the energy separation mechanism using code system Fluent. They observed that the standard k- $\epsilon$  turbulence model predicted the velocity and temperature separation better than the RNG k- $\epsilon$  turbulence model. Skye et al. [3] also reported similar results. Eiamsa-ard and Promvonge [12] used a mathematical model for the simulation of energy separation effect. They used the ASM and k- $\epsilon$  turbulence model and concluded that the diffusive transport of mean kinetic energy had a substantial influence on energy separation. H. Khazaei et al. [14] demonstrates about energy separation effects in a vortex tube using a CFD model. The effects of varying the geometry of vortex tube components, such as hot outlet and diameter size, on tube performance, have been studied, besides using different gases as a working medium in a vortex tube. Rahim Shamsoddini et al. [15], deals on the effects of the nozzles number on the flow and power of cooling of a vortex tube using a three-dimensional numerical fluid dynamic model. They observed that as the number of nozzles increased, power of cooling increases significantly while cold outlet temperature decreases moderately. H. Pourariaa et al. [16] indicated that an increase in divergent tube angle results in an increase in cooling performance of vortex tube. However, there is a critical divergence angle, so that further increase

Million Asfaw Belay, Lecturer, Bahirdar Institute of Technology, Bahirdar University, Bahirdar, Ethiopia.

will lead to reduction in cooling performance of the device. Tanvir Farouk et al. [13] used the CFD-ACE+ code to predict the energy separation. They used the large eddy simulation (LES) technique to model the turbulence and compared the predicted results with the published experimental results (Skye et al.) and  $k-\epsilon$  predictions. They observed that temperature separation predicted by the LES was closer to the experimental results. However, the vortex tube dimensions and inlet boundary condition used in the LES model are significantly different from those used in the experiment. Also they used LES technique for predicting the gas flow and temperature fields and the species mass fractions (nitrogen and helium) in the vortex tube. Hence, there should be a tradeoff between accuracy and computational expenses. If reasonable accuracy is obtained with a lower order turbulence model, then it can be used for design purpose the model is shown in Fig 1.

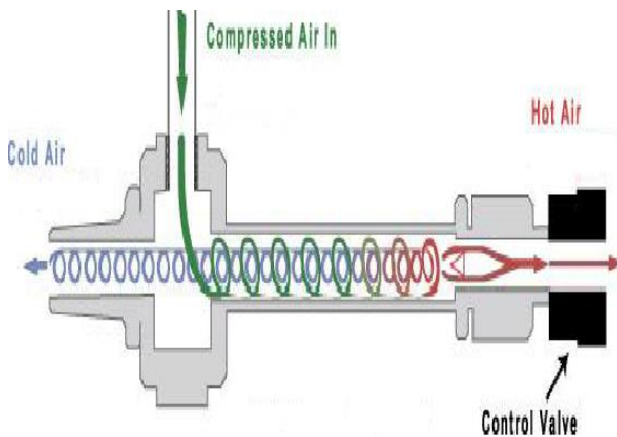


Fig. 1 The fluid flow inside a vortex tube

From this literature review it is observed that none of the researchers performed a three dimensional numerical simulation of vortex tube using LES turbulence model. Thus, the main motivation of this paper is a three dimensional vortex tube with a high pressure inlet boundary condition (400kPa) and a low pressure inlet boundary condition (200kPa) using different type of CFD models including LES to compare the fluid flow and temperature separation so that a computationally less expensive suitable turbulence model can be chosen for the simulation of vortex tube. The models that are used in this work are Reynolds average Navier–Stokes (RANS) based turbulence models (i.e., standard  $k-\epsilon$ , RNG  $k-\epsilon$  and  $k-\omega$ ) and more advanced turbulence models (i.e., RSM and LES). The primary and fundamental objectives of this research work are; to determine a temperature separation and a fundamental understanding of the fluid dynamics and thermodynamics of the primary and secondary flows in the vortex tube, to investigate the performance curve, to compare and contrast the temperature separation and flow field along the VT of five turbulence models, to locate the position of stagnation point and secondary flow in VT, to identify the major reason for temperature separation and its mechanism, to study the vortex tube characteristics by observing the pressure, velocity and temperature fields, and the results from the turbulence models are analyzed and compared to establish how accurate they are at computing this type of flow field.

II. CFD MODELING

2.1. Geometry of Model

The computational domain used for this simulations (Table 1) is similar to that of the past study of Skye et al. [3].

(1) Table 1 Geometric summary of CFD models used for vortex tube

Measurements	Skye's experimental vortex tube	Present vortex tube with 6 number of straight nozzle
Working tube length (L)	100mm	100mm
Working tube diameter (D)	20mm	20mm
Nozzle height	3mm	3mm
Nozzle width	3mm	3mm
Nozzle length ( $L_N$ )	15mm	15mm
Hot exit area	113 mm <sup>2</sup>	113mm <sup>2</sup>
Cold exit diameter ( $d_c$ )	6mm	6mm

A Commercial RHVT has a lot of components. However, for the purposes of CFD analysis, this shape can be resolved down to a very simple model without the loss of the most important aspects of the device. The basic elements of the vortex tube which is similar to that of the past study of Skye et al. [3] for CFD analysis are shown on the Fig. 2.

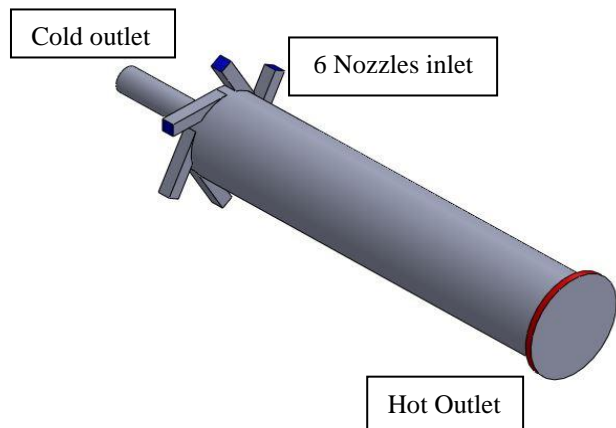


Fig. 2 Isometric view of RHVT

A 100mm working tube length was used as the boundary geometry for the CFD model. The hot and cold tubes are of circumferential shape with exit areas of 113mm<sup>2</sup> and 28mm<sup>2</sup> respectively. The main part of the vortex tube called the generator plays an important role in the generation of the cooler temperature stream. The vortex tube consists of 6 rectangle shaped nozzles. The nozzles were oriented tangential around the periphery of the generator. The width, length and height of each nozzle

2.2 Governing equations

The compressible turbulent flows in the vortex tube are

governed by;

Conservation of Mass:

$$\frac{\partial \rho}{\partial t} + \nabla \cdot (\rho \vec{V}) = 0 \quad (1)$$

Conservation of Momentum

$$\frac{\partial (\rho \vec{V})}{\partial t} + \nabla \cdot (\rho \vec{V} \vec{V}) = -\nabla P + \nabla \cdot (\tau) \quad (2)$$

Conservation of Energy

$$\frac{\partial (\rho h)}{\partial t} + \nabla \cdot (\rho u h) = \frac{\partial P}{\partial t} + \nabla \cdot \left( \frac{k}{c_p} \nabla h \right) - \nabla \cdot (\tau \cdot \vec{V}) \quad (3)$$

$$\text{State equation } P = \rho RT \quad (4)$$

### 2.3 Assumptions and Boundary Conditions

Basic assumptions involved for all computational turbulence models for analysis of vortex-tube are compressible flow, steady or transient (specifically for LES turbulence model), turbulent, subsonic three dimension flow with uniform fluid properties at the inlet. The compressible fluid is treated as an ideal gas. This paper focused on high and low pressure inlet boundary conditions for all type of turbulent models to identify the effects of inlet pressure on the fluid field and temperature separation. In the inlet region, pressure boundary condition of the vortex tube with inlet pressure 400 kPa for high pressure inlet condition and 200 kPa for low pressure inlet condition and a total temperature of 300 K is defined (Table 2). The inlet region consists of 6 nozzles. The hot outlet is considered as circumferential outlet.

In the computational domain as shown in Fig. 2 the air enters the vortex tube through the nozzles with a tangential velocity. Pressure outlet is the recommended boundary condition at outlet for an ideal gas in turbulent flow, which was adopted in this work at the cold and hot outlets. Atmospheric pressure was specified at the cold exit of the vortex tube. The pressure boundary condition at the hot exit was varied to control the mass flow rates among the two exits shown at Table 2. The temperature at the hot and cold exits was assigned a zero gradient boundary condition. The tube walls were considered to be adiabatic with no slip boundary condition for the velocity components.

Table 2 Variable and fixed parameters for the vortex tube simulations

Case	Fixed parameters		Variable parameters
	Inlet pressure (kPa)	Cold exit pressure (kPa)	Hot exit pressure (kPa)
1	400	101.325	105
2			60
3			70
4			80
5			90
6			100
7			110
8			115
9			200

### 2.4 Grid independence study

A mesh convergence study focusing on cold temperature outputs of the RHVT was conducted. This study was carried out in order to ascertain a mesh density such that any potential increase in the number of elements/nodes above the largest solved mesh density would yield a marginal increase in accuracy of CFD results, insufficient to warrant any increase in mesh density. This final mesh density was then used with confidence for comparative studies of other factors such as choice of turbulence model and changes the inlet pressure of the RHVT.

For case 1 with hot exit pressure 105 kPa, grid independence tests were carried out for several grid designs. Initially the k-ε turbulence model is utilized to perform a mesh element density convergence study with the cold temperature outputs of the vortex tube as the measured criteria. The variation of the key parameters such as the cold temperature difference for different cell volumes was investigated. Investigations of the mesh density showed that the model predictions are insensitive to the number of grids above 500,000 (Fig. 3). Once mesh independent test is established additional turbulence models such as the RNG k-ε, k-ω and RSM are run on this mesh to ascertain the performance of each turbulence model. But LES needs more fined type of mesh than others so that it has an accurate result with the experiment one.

Therefore, a hexahedral mesh consisting of 550,000 grid elements (Fig. 4) was used for turbulence models of sk-ε, RNGk-ε, k-ω and RSM to produce the results shown in this work. Since LES turbulent model is more sensitive to mesh element the finer grid element (1,000,000 grid elements) is necessary to determine the better fluid flow and temperature separation. The mesh is finer in regions where large gradients in velocity or pressure are expected, specifically the inlet plane, the vortex region and hot & cold exits.

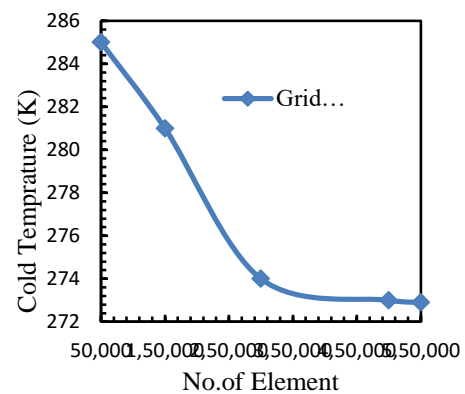


Fig. 3 Grid independence study on the cold temperature side



Fig. 4 Hexahedral mesh of three dimensional model of vortex tube

2.5 Solution procedures

After successfully accomplished the geometry and mesh of vortex tube the next step was solving Navier-stokes equations and energy equations using finite-volume method (using Fluent code) together with the relevant turbulence model equations.

For sk- $\epsilon$ , RNG k- $\epsilon$ , k- $\omega$  and RSM the simple algorithm was selected for pressure-velocity decoupling. The discretization of the governing equations is accomplished by a first-order upwind scheme. The air entering the tube is modeled as an ideal gas of constant specific heat capacity, thermal conductivity, and viscosity. Due to the highly non-linear and coupled features of the governing equations for swirling flows, low under-relaxation factor 0.2 was used for pressure, momentum, turbulent kinetic energy and energy, to ensure the stability and convergence. The convergence criterion for the residual was set as  $1 \times 10^{-5}$  for all equations.

For transient LES turbulence model simple algorithm are used for pressure-velocity decoupling. For the convective-diffusive terms in the mass, momentum and energy conservation equations a second-order upwind scheme [17] is used. The Kolmogorov time scale calculated from the micro scale relations was found to be  $2 \times 10^{-4}$  s. A  $10 \mu\text{s}$  time-step size with 50,000 number of time step was chosen, which is smaller than the Kolmogorov time scale. The implicit

calculations within a given time-step are continued until the variation in the variables is within  $10^{-05}\%$  of the value of the variable from the previous iteration. The time marching calculations were terminated when a pseudo steady-state behavior was observed.

III. RESULTS AND DISCUSSION

This section focused on the pressure contour, temperature contour, velocity contour of the vortex tube and the velocity field at  $x/L=0.5$  of the vortex tube with different turbulence model. To simplify the study we categories it in to two parts i.e., for high pressure inlet boundary condition (400 kPa) and low pressure inlet boundary condition (200 kPa).

3.1 Thermal performance

3.1.1 High pressure inlet boundary condition

The vortex tube characteristics for 400 kPa inlet pressure, 101 kPa cold exit pressure and 105 kPa hot exit pressure have been studied by observing the temperature, pressure and velocity fields (Figs. 5- 7) using the five turbulence models mentioned in the previous section.

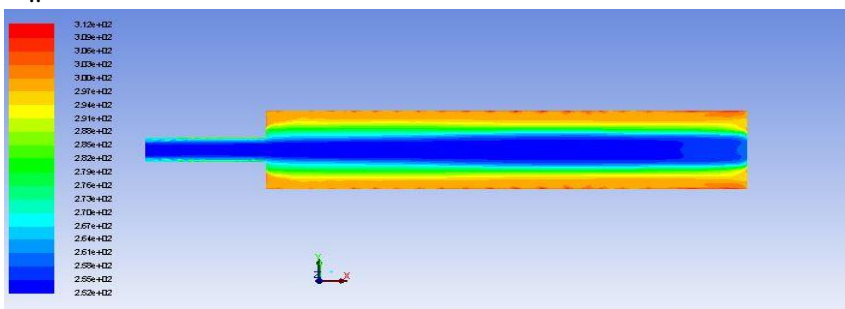


Fig. 5 Total temperature distributions (K) for numerical simulation results in the vortex tube, LES Model

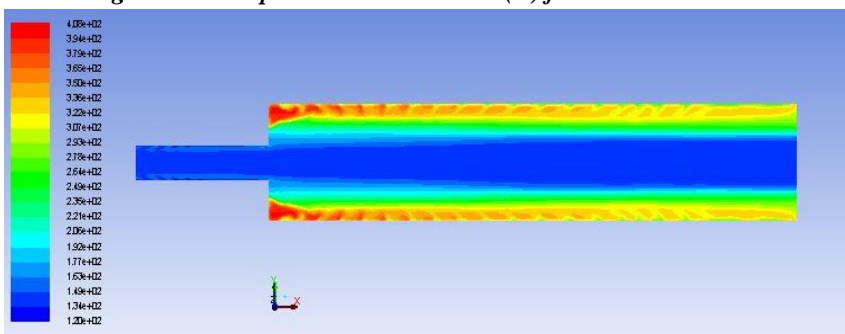
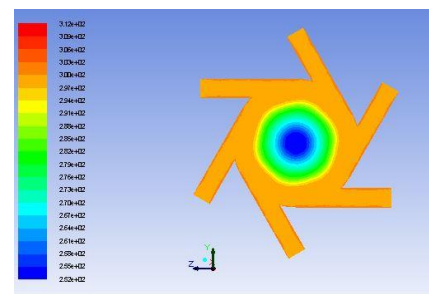


Fig. 6 Total pressure distributions (kPa) for numerical simulation results in the vortex tube, LES model

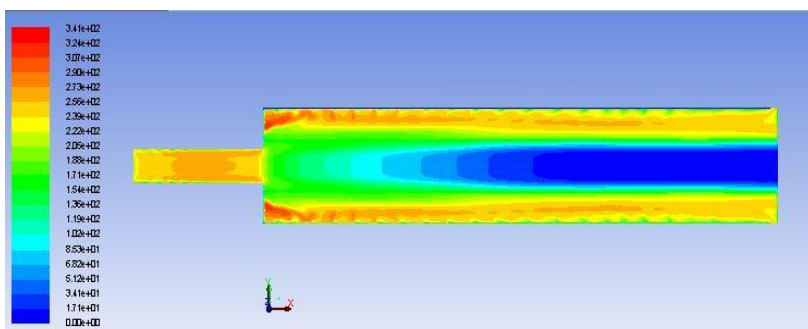
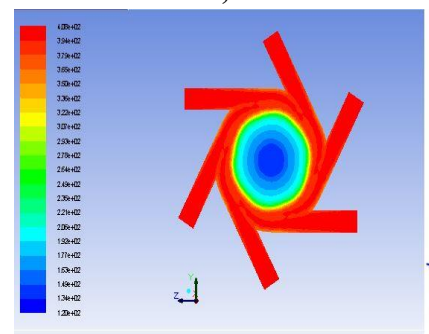


Fig. 7 Total velocity distributions (m/s) for numerical simulation results in the vortex tube, LES model

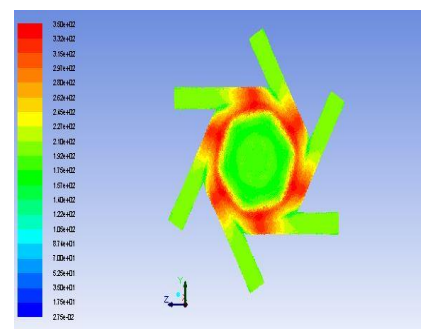


Table 3 Hot and cold temperature (K) comparisons' of CFD models with experiment (case 1)

Temperature (K)	Turbulence model					Sky's et al. experiment
	sk-ε	RNG k-ε	k-ω	RSM	LES	
T <sub>c</sub>	267	274	266	268	261	256
T <sub>h</sub>	312	309	310	315	312	317
T <sub>c</sub> Deviation	11	18	10	12	5	-
Number of cores	14	14	14	14	14	-
CPU time	4hr	4-5hr	4hr	5hr	2 weeks	-

From Table 3, in standard k-ε model a difference of 45 K in total temperature between the hot and the cold outlet is obtained with T<sub>h</sub> 312 K and T<sub>c</sub> 267 K. For RNG k-ε model the total temperature of 34 K is obtained with T<sub>h</sub> 309 K and T<sub>c</sub> 274 K. This shows that the span of the lower temperature region is greater than standard k-ε model which means there is a lower level of mixing predicted by the model. A temperature distribution for k-ω model describes with total temperature separation of 44 K is obtained T<sub>h</sub> 310 K and T<sub>c</sub> 266 K at hot and cold exits respectively. For advanced numerical model of RSM model, total temperature distribution of 47 K is obtained with T<sub>h</sub> 315 K and T<sub>c</sub> 268 K at hot and cold exits respectively. Thus, we can conclude that the total temperature distributions obtained by k-ω model and RSM have quite similar with that of standard k-ε model. For transient turbulence model of LES model, Compared to other turbulence models the highest temperature separation obtained with total temperature of 51 K which contains T<sub>h</sub> 312 K and T<sub>c</sub> 261 K. Although due to fine mesh element and small time step used in LES, the CPU time is greater than other turbulence models.

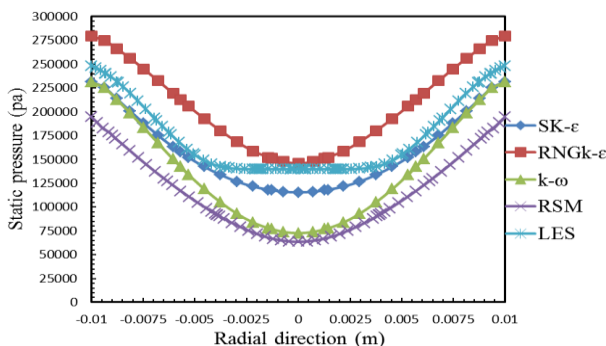


Fig. 8 Radial distribution of static pressure (Pa) at x/L = 0.5

The flow characteristics and temperature separation inside the vortex tube have been studied by observing the pressure, velocity and temperature fields using the five turbulence models mentioned in the previous section. A radial distribution of static pressure gradient is observed on Fig. 8 at x/L = 0.5 with a higher pressure value at the wall. The strong swirling flow inside the vortex tube causes the expansion of air from the periphery to the core. This pressure differential between the periphery and the core obtained with the LES model is minimum (108.2 kPa), and while the pressure drop

obtained with the k-ω is much higher (158.6 kPa) than that obtained with the other turbulence models. It is also observed that the gradients are smaller in the prediction with LES model. Thus, the LES model predicts a higher level of turbulence and mixing.

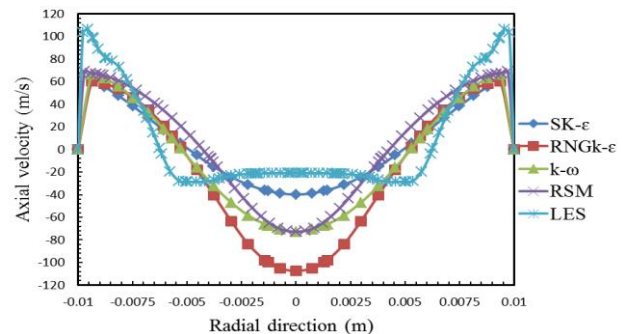


Fig. 9 Radial distribution of axial velocity (m/s) at x/L = 0.5

Fig. 9 shows the radial distribution of axial velocity at x/L = 0.5. A reverse flow phenomenon in the vortex tube is clearly observed in this figure. For all five turbulence models the axial velocity profiles obtained at peripheral region have similar quantitative nature. The positions of zero axial velocity along radial locations are also observed which is very close for all turbulence models. But, compared to LES model the axial velocity is observed to decrease rapidly towards the core region for RNG k-ε model. The total magnitude of the axial velocity observed at the core region of the vortex tube with the RNG k-ε model is 107 m/s, which is higher than the values of other four turbulence models. This indicates there is a weaker mixing in the flow and significantly low level of turbulence predicted by the RNG k-ε model.

The dominant velocity component in the vortex tube is swirl velocity that has a major role in temperature separation and flow field analysis. The radial distribution of swirl velocity is shown in Fig. 10. The steep swirl velocity gradient near the core region shows that there is a greater amount of tangential shear stress in that region. Thus, It may be noted that the most important mechanism for the energy separation in a vortex tube is tangential shear work [4]. A free vortex flow is observed near the core region while forced vortex flow is predominantly formed in the rest of the tube. It is also observed that LES model have a maximum swirl velocity component near the wall region than that obtained with other turbulence models.

Figure 11 shows the radial distribution of radial velocity at  $x/L = 0.5$ . The magnitude of the radial velocity component is much smaller compared to the other components. A negative value of the radial velocity means the flow direction in the vortex tube is radially inward. For RNG  $k-\epsilon$  model a radial velocity component profile has a significant deviation near the core region compared to other turbulence models. This may indicate that there is lower level of turbulence predicted by the RNG  $k-\epsilon$  model near the core region.

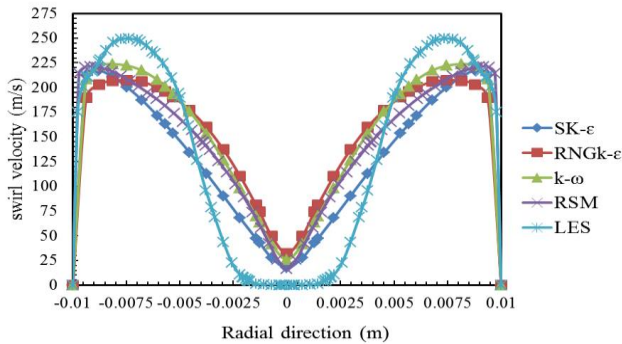


Fig. 10 Radial distribution of swirl velocity (m/s) at  $x/L = 0.5$

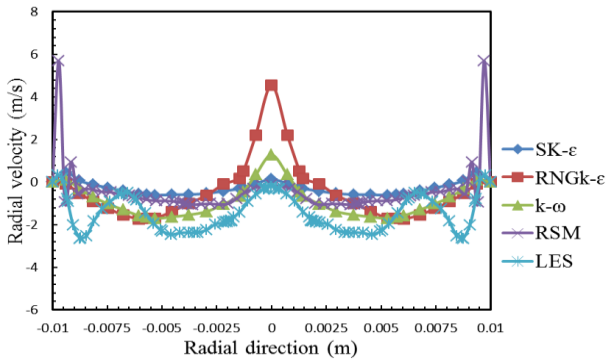


Fig. 11 Radial distribution of radial velocity (m/s) at  $x/L = 0.5$

Figure 12 shows the radial distribution of static temperature at  $x/L = 0.5$ . It observed the Static temperature is decrease sharply near to the periphery boundary layer followed by fairly constant with radial direction. Aljuwayhel et al.[4] also stated similar thing regarding to static temperature distribution. As it observed from Fig. 12 for all turbulence models the static temperature profiles have similar qualitative nature, the static temperatures at the periphery and the core region and the static temperature differentials between the periphery and the core are observed to be considerably different.

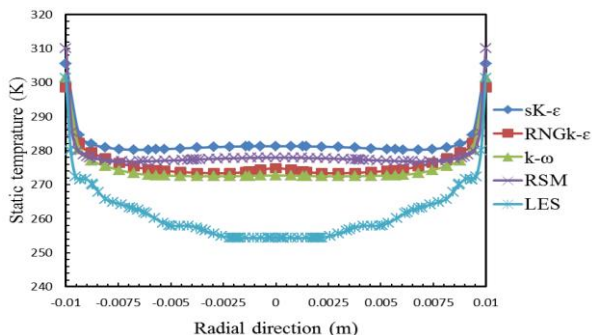


Fig. 12 Radial distribution of static temperature (K) at  $x/L = 0.5$

The static temperature differentials between the periphery and the core predicted by RNG  $k-\epsilon$  model,  $k-\omega$  model, RSM model, and LES model are 28 K, 28.6 K, 32 and 46.9, respectively, which are higher than standard  $k-\epsilon$  model with value of 23.7 K. These differentials for different turbulence models have contribution for variation in the pressure gradient between the periphery and the core with in these turbulence models which have a big role on the level of turbulent mixing (Fig. 8).

It has been observed that the greater temperature differential is due to the higher pressure drop. Also, lower the static pressure at the core region would cause for lower static temperature at that location. So, it concludes that the static temperature drop can be described as a result of the radial expansion of air in the vortex tube.

The radial distribution of total temperature at  $x/L = 0.5$  is presented in Fig. 13. The total temperature profiles is the sum of the constant static pressure profiles (Fig. 8) and swirl velocity (tangential velocity) profiles (Fig. 10). Static temperature is calculated from static enthalpy while total temperature is outcomes from total enthalpy, which consists of both kinetic energy and static enthalpy.

The dominance of strongly swirling flow inside the vortex tube causes the expansion of air from the periphery to the core region, which causes for reducing the static pressure and static temperature near the core. Generally the distribution of static pressure is determined by the distribution of static temperature while the swirl velocity component, determines the distribution of the kinetic energy and total enthalpy inside the vortex tube.

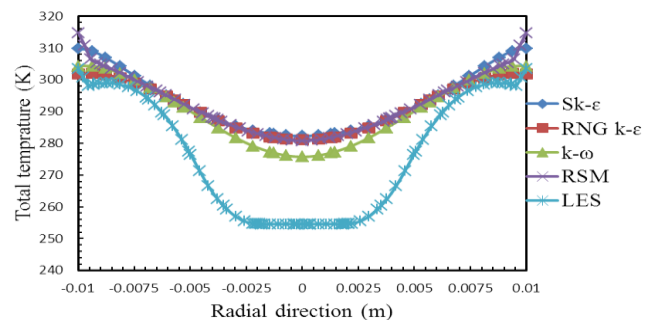


Fig. 13 Radial distribution of total temperature (K)

Basically the total temperature profile follows the swirl velocity profile since the static temperature is fairly constant in the radial direction except near the wall. Thus, consistency of the total temperature profile with the profiles of static pressure and swirl velocity indicates that the temperature separation between the peripheral and inner fluid layers is due to a combination of the radial expansion of air and the change in kinetic energy. Due to the shear work done by the inner fluid layers on the peripheral layers, fluid in the core region possesses lower kinetic energy, thereby lowering the total enthalpy and total temperature.

Although all turbulence models have similar qualitative nature of the total temperature profiles, the total temperatures at the periphery and the core and the total temperature differential between them have different quantitative value for each of these turbulence models. The total temperature differential between the periphery and the core region obtained with the LES model (48.8 K) is relatively higher than other turbulence models. This variation with different

turbulence models have a big contribution to the variation in the levels of turbulence predicted by the models.

The temperature separation obtained from the present standard k- $\epsilon$ , Farouk et.al. LES and 3-D LES calculations were compared with experimental result of Skye et al [3] for validation. As seen in Fig. 14, the cold exit temperature separations predicted by the models are in good agreement with the experimental results. Also we conclude that the cold temperature separation calculated by LES turbulent model of 3-D VT is better than other models shown on Fig. 14. The cold exit temperature difference is observed to decrease with an increase in the cold mass fraction. Thus the maximum cold temperature difference was observed in the cold mass fraction range of 0.2 to 0.4

### 3.1.2 Low pressure inlet boundary condition

In this section a vortex tube characteristics for 200 kPa inlet pressure, 101.325 kPa cold exit pressure and 105 kPa hot exit pressure boundary conditions have been studied by observing the temperature, pressure and velocity fields (Figs. 15 -17) using the five turbulence models mentioned in the previous section.

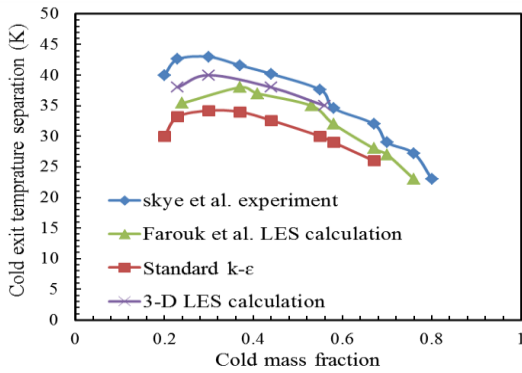


Fig. 14 Cold exit temperature separation ( $T_i - T_c$ ) as a function of cold mass fraction

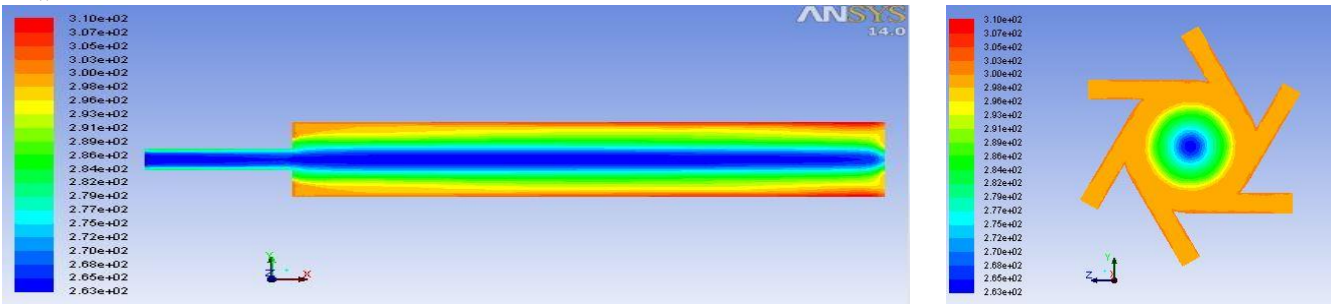


Fig.15 Total temperature distributions (K) for numerical simulation results for in the vortex tube, LES model

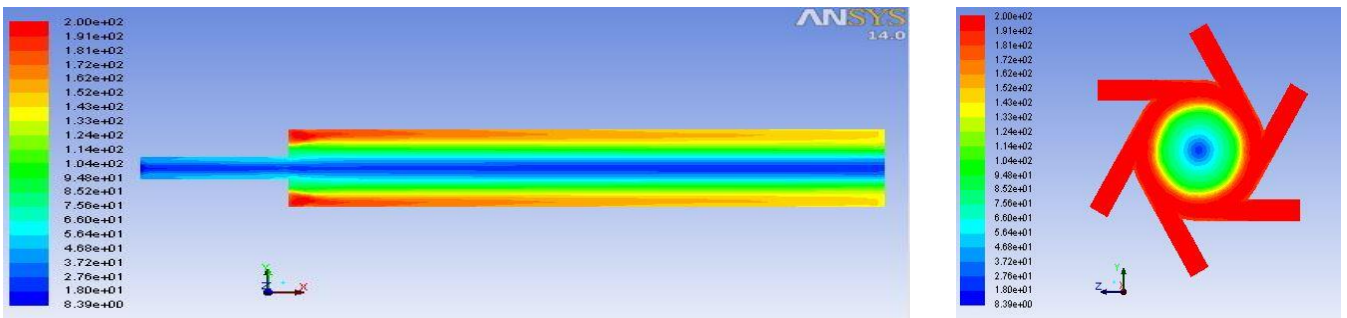


Fig. 16 Total pressure distributions (kPa) for numerical simulation results in the vortex tube, LES model

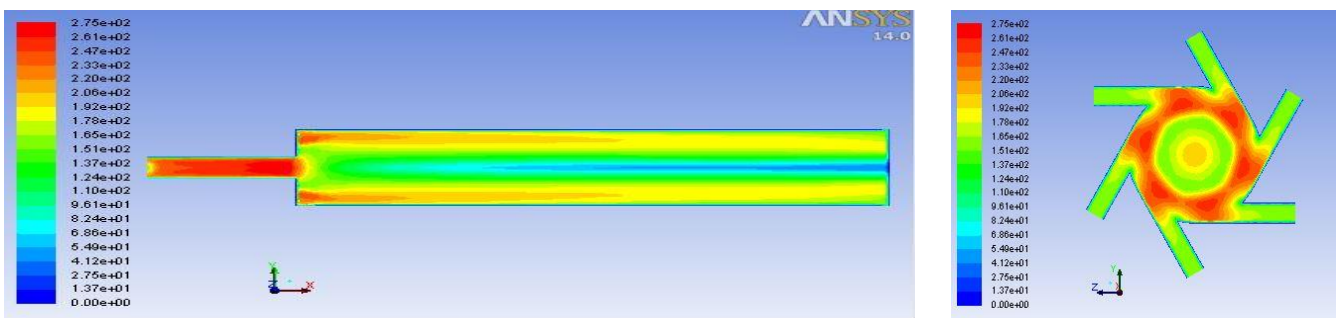


Fig.17 Total velocity distributions (m/s) for numerical simulation results in the vortex tube, LES model

Figure 15, Figure 16 and Figure 17 shows the total temperature, total pressure and total velocity distribution for case 9 (Table 4.2) in the vortex tube with the standard  $k-\epsilon$  model, RNG  $k-\epsilon$ ,  $k-\omega$ , RSM and LES respectively. The phenomenon of temperature separation is also clearly observed in these figures. From Table 4.4, in standard  $k-\epsilon$  model a difference of 30 K in total temperature between the hot and the cold outlet is obtained with  $T_h$  310 K and  $T_c$  280 K. In RNG  $k-\epsilon$  a total temperature separation of 21 K is obtained in this case with  $T_h$  308 K and  $T_c$  287 K. From the total temperature distribution with  $k-\omega$  model total temperature separation of 29 K is obtained with  $T_h$  309 K and  $T_c$  280 K. From the total temperature distribution with the RSM model, total temperature separation of 33 K is obtained with  $T_h$  314 K and  $T_c$  281 K. Thus, the total temperature distributions obtained with the  $k-\omega$  model and RSM appear to be quite similar to that obtained with standard  $k-\epsilon$  model. From the total temperature distribution with the LES model, total temperature separation of 47 K is obtained with  $T_h$  310 K and  $T_c$  273 K which is the highest temperature separation than other turbulence models.

For low pressure inlet boundary condition the pressure, velocity and temperature fields have similar qualitative nature with high pressure inlet boundary condition for all turbulence models. Thus to avoid the redundancy of those plots and explanations not included in this section. Generally, the magnitude of the calculated temperature separation depends on the magnitude of inlet boundary condition.

### 3.2. Flow field

In this section the numerical results of this CFD study of the RHVT is to quantify the influence of secondary flow within the tube. Before concluding its influence, this secondary flow had to be captured clear numerically; stagnation point location exists within the RHVT, as can be seen in Fig. 18 and it can be seen that a region of recirculating secondary flow is presented within the RHVT.

Figure 18 shows the streamlines in the  $x-y$  plane associated with the flow inside the vortex tube. Notice that the interaction between the gas streams leaving the cold and hot ends with a significant distance before the exits. Therefore, in the CFD model the majority of power separation occurs before this point as noted by Aljuwayhel et al. [4].

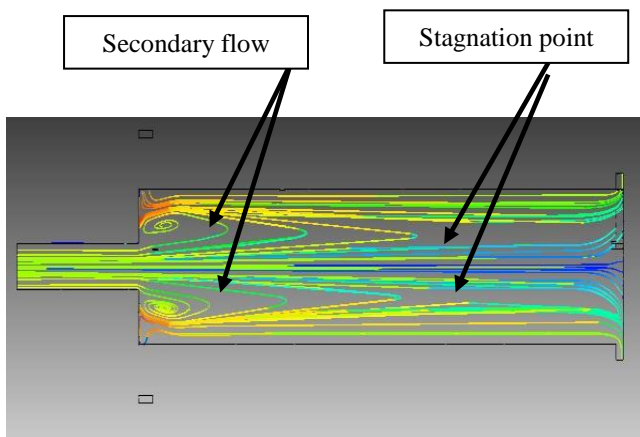


Fig. 18 Predicted Streamlines plot with secondary flow for the vortex tube in  $x-y$  plane (case 1)

The stagnation point position within the vortex tube can be determined based on velocity profile along the tube length at the point, where it ceases to a negative value. Figure 18 shows the stagnation point and corresponding streamlines in the  $x-y$  plane.

From the computed velocity fields, Streamline for two specific fluid elements that exit the flow field via the cold and hot exits, is shown in Fig. 19. The fluid element that leaves by the cold exit advances towards the end of the vortex tube with a swirling motion. The flow direction however reverses near the tube end and the particle starts moving towards the cold exit, without reversing the direction of rotation. As the particle starts moving towards the cold exit, the swirling motion was found to decrease. Also this Figure depicts the streamline of a fluid element that exits via the hot exit. After entering the tube the particle advances towards the hot exit with a swirling motion.

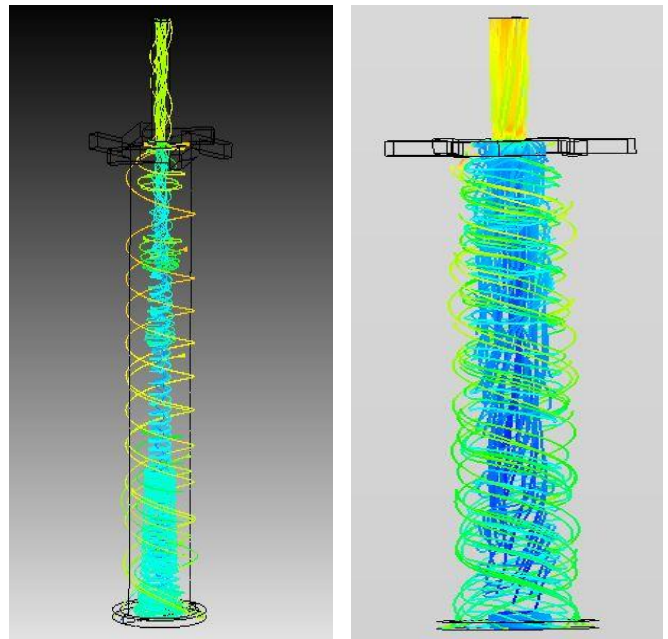


Fig. 19 Streamline for the inner core and for the outer peripheral fluid flow in the entire vortex tube in three-dimensional space (case 1)

## IV. CONCLUSION

The computed temperature separation and flow fields are compared favorably to Skye's experimental results and have shown that the utilized Fluent 14.0 software is capable of calculating the following; the temperature, pressure and velocity distribution, the Static and total temperature profile, the static pressure profile, the axial, tangential and radial velocity profile, cold and hot outlet total temperature separation, confirmation of the presence of secondary flow, and confirmation of a location of a stagnation point in the flow. The numerical model is also capable of predicting temperature and flow field inside the vortex tube as well as the temperature separation effect that is consistent with the observed behavior. Predicted results show that energy separation occurs mainly due to transfer of loss of angular momentum as a form of heat from the inner vortex to the outer vortex. Results also revealed that the better energy separation observed when the simulation was carried out using LES turbulence model.

## REFERENCES

- [1] G. Ranque, Experiments on expansion in a vortex with simultaneous exhaust of hot air and cold air, *J Phys Radium (Paris)*, 4 (1933) 112-114.
- [2] R. Hilsch, The use of the expansion of gases in a centrifugal field as cooling process, *Review of Scientific Instruments*, 18 (1947) 108-113.
- [3] H. Skye, G. Nellis, and S. Klein, Comparison of CFD analysis to empirical data in a commercial vortex tube, *International Journal of Refrigeration*, 29 (2006) 71-80.
- [4] N.F. Aljuwayhel, G.F. Nellis, and S.A. Klein, Parametric and internal study of the vortex tube using a CFD model, *International Journal of Refrigeration-Revue Internationale Du Froid*, 28 (2005) 442-450.
- [5] G. Scheper, The vortex tube: internal flow data and a heat transfer theory, *Refrigerating Engineering*, 59 (1951) 985-989.
- [6] V. Martynovskii and V. Alekseev, Investigation of the vortex thermal separation effect for gases and vapors, *Sov Phys-Tech Phys*, 26 (1957) 2233-2243.
- [7] H. Bruun, Experimental investigation of the energy separation in vortex tubes, *Journal of Mechanical Engineering Science*, 11 (1969) 567-582.
- [8] Y. Xue, M. Arjomandi, and R. Kelso, A critical review of temperature separation in a vortex tube, *Experimental Thermal and Fluid Science*, 34 (2010) 1367-1374.
- [9] P. Promvonge, A numerical study of vortex tubes with an algebraic Reynolds stress model, Ph.D. thesis, University of London, United Kingdom, 1997.
- [10] W. Frohlingdorf and H. Unger, Numerical investigations of the compressible flow and the energy separation in the Ranque-Hilsch vortex tube, *International Journal of Heat and Mass Transfer*, 42 (1999) 415-422.
- [11] U. Behera, P. Paul, S. Kasthuriangan, R. Karunanithi, S. Ram, K. Dinesh, and S. Jacob, CFD analysis and experimental investigations towards optimizing the parameters of Ranque-Hilsch vortex tube, *International Journal of Heat and Mass Transfer*, 48 (2005) 1961-1973.
- [12] S. Eiamsa-Ard and P. Promvonge, Numerical investigation of the thermal separation in a Ranque-Hilsch vortex tube, *International Journal of Heat and Mass Transfer*, 50 (2007) 821-832.
- [13] T. Farouk and B. Farouk, Large eddy simulations of the flow field and temperature separation in the Ranque-Hilsch vortex tube, *International Journal of Heat and Mass Transfer*, 50 (2007) 4724-4735.
- [14] H. Khazaei, A. Teymourtash, and M. Malek-Jafarian, Effects of gas properties and geometrical parameters on performance of a vortex tube, *Scientia Iranica*, 19 (2012) 454-462.
- [15] R. Shamsoddini and A.H. Nezhad, Numerical analysis of the effects of nozzles number on the flow and power of cooling of a vortex tube, *International Journal of Refrigeration*, 33 (2010) 774-782.
- [16] H. Pouraria and M. Zangoee, Numerical investigation of vortex tube refrigerator with a divergent hot tube, *Energy Procedia*, 14 (2012) 1554-1559.
- [17] B. Leonard, Convection-diffusion algorithms, *Advances in numerical heat transfer*, (1997).
- [18] Y. Wu, Y. Ding, Y. Ji, C. Ma, and M. Ge, Modification and experimental research on vortex tube, *International Journal of Refrigeration*, 30 (2007) 1042-1049.



**Million Asfaw**, Lecturer and Chair of Thermal Engineering department at the Faculty of Mechanical and Industrial Engineering in Bahir Dar University, with BSc. in Mechanical Engineering at Bahir Dar University and MSc. in Mechanical Engineering specialized on Thermal Science and Fluid Mechanics at National Taiwan University of Science and Technology, Taiwan.